IJARSCT
International Journal of Advanced Research in Science, Communication and Technology
International Open-Access, Double-Blind, Peer-Reviewed, Refereed, Multidisciplinary Online Journal
ISSN: 2581-9429
Volume 5, Issue 3, July 2025
Impact Factor: 7.67

Antioxidant and Antimicrobial Activity of Pure and Ag-Doped $CuFe_2O_4$ Nanoparticles Prepared by Microwave-Assisted Green Synthesis

Sunil P. Gawali[a,b*] and D. V. Mane[c,d]

[a]Department of Chemistry, Sundarrao More Arts, Commerce and Science College, Poladpur, Raigad, India
[b]School of science, Yashwantrao Chavan Maharashtra open University, Nashik, Maharashtra, India
[c]Former. Regional Director, YCMOU Nashik, India
[d]Department of Chemistry, Shri Chhatrapati Shivaji College Omerga, Dharashiv, India

Abstract: *This investigation demonstrates the successful fabrication of silver-substituted copper ferrite nanoparticles (AgxCu1-xFe2O4, where x = 0.05, 0.1, 0.2) through microwave-assisted biosynthesis utilizing Asteracantha longifolia leaf extract as both reducing and stabilizing agent. X-ray diffraction analysis confirmed single-phase cubic spinel structures with lattice parameters ranging from 8.294 to 8.165 Å. Electron microscopy revealed morphological transitions from spherical to irregular geometries with crystallite sizes between 15.43 and 18.85 nm. Enhanced optical absorption in the UV-visible region (300-800 nm) resulted from surface plasmon resonance effects of silver nanodomains. Magnetic characterization showed decreased saturation magnetization correlating with silver content, attributed to diamagnetic Ag^+ ions disrupting magnetic exchange interactions. Thermal analysis indicated structural stability up to 600°C with minimal mass loss. Antioxidant evaluation through DPPH radical scavenging demonstrated concentration-dependent activity enhancement, with AgxCu1-xFe2O4 exhibiting 55.35% radical neutralization efficiency compared to 41.87% for undoped copper ferrite.*

Keywords: Microwave, sol-gel, Ferrite, X-ray diffraction, HRTEM, Antimicrobial activity

I. INTRODUCTION

Spinel ferrite nanoparticles represent a class of nanocrystalline materials attracting considerable scientific attention due to their unique combination of magnetic, electrical, and catalytic properties [1]. Copper ferrite ($CuFe_2O_4$) nanostructures exhibit exceptional magnetoelectrical characteristics coupled with robust catalytic functionality, demonstrating remarkable thermodynamic stability and chemical resistance under extreme operational conditions [2, 3]. These properties make them suitable for applications including magnetic data storage, catalysis, ferrofluids, biosensors, and environmental remediation. Contemporary synthetic approaches for spinel-type compounds encompass various methodologies including coprecipitation, solvothermal crystallization, lyophilization techniques, microemulsion templating, and sol-gel polymerization protocols. Among these methods, microwave-assisted sol-gel auto-combustion using citric acid as fuel presents a particularly effective route for generating monodisperse nanocrystalline particles under moderate thermal conditions. This approach offers sustainable alternatives that minimize dependency on expensive reagents and toxic precursors while reducing energy consumption. *Asteracantha longifolia*, a medicinally significant species in traditional Ayurvedic pharmacopeia, contains abundant bioactive metabolites including fatty acid esters, mineral cofactors, polyphenolic antioxidants, proanthocyanidin oligomers [4], nitrogenous alkaloids [5], enzymatic proteins[6], amino acid residues [7], terpenoid compounds [8], vitamin complexes [9], and glycosidic derivatives [10]. These constituents confer therapeutic properties against various disorders and provide antifungal, cytotoxic, anti-inflammatory, antipyretic, antioxidant, insecticidal, hepatoprotective, immunomodulatory, antiplatelet, and antiviral bioactivities. Previous investigations have demonstrated the potential of plant extracts for metallic nanoparticle fabrication [11-13]. However, research concerning microwave-assisted synthesis of pristine and silver-modified copper ferrite nanomaterials utilizing *Asteracantha longifolia* foliar extracts remains limited. This

IJARSCT
International Journal of Advanced Research in Science, Communication and Technology
International Open-Access, Double-Blind, Peer-Reviewed, Refereed, Multidisciplinary Online Journal
ISSN: 2581-9429
Volume 5, Issue 3, July 2025
Impact Factor: 7.67

investigation addresses this gap, focusing on the controlled fabrication of Ag-$CuFe_2O_4$ and $CuFe_2O_4$ nanoparticles possessing distinctive microstructural architectures and enhanced physicochemical properties [14].

II. MATERIALS AND METHODS

2.1 Plant Material Collection and Extract Preparation

Fresh *Asteracantha longifolia* leaves were collected from Mahad city, Raigad, Maharashtra. The leaves were thoroughly cleaned under tap water, washed with double-distilled water, and dried for four days under shade conditions. After drying, the leaves were ground using mortar and pestle and stored in an airtight bottle.

Figure 1 Dried and processed *A. longifolia* leaves prepared for aqueous extraction. Images were captured in Cholai, Maharashtra, India (GPS coordinates: 17°9'12" N, 73°46'8" E)

For extract preparation, 20 g of powdered plant material was added to a 500 mL flask containing 200 mL of water. The mixture was heated for three minutes in a microwave at 350-watt power, followed by 30 minutes of ultrasound treatment. The aqueous extract was filtered using Whatman No. 41 filter paper and stored in a refrigerator for subsequent use.

2.2 Biosynthesis of Copper Ferrite Nanoparticles

$CuFe_2O_4$ nanoparticles were synthesized using microwave-assisted sol-gel auto-combustion method with citric acid as fuel in the presence of *A. longifolia* leaf extract. Precursor materials $Cu(NO_3)_2 \cdot 3H_2O$, $Fe(NO_3)_3 \cdot 9H_2O$, and citric acid (metal salt to citric acid ratio of 1:3) were completely dissolved in 50 mL of deionized water separately. Subsequently, 20 mL of *A. longifolia* leaf extract was added. Ammonium hydroxide was added dropwise to adjust the pH to 7. The mixed solution was placed in a microwave oven and heated with magnetic stirring at 80°C until gel formation occurred. The obtained gel was continuously heated and stirred at 140°C in the microwave, leading to spontaneous combustion and ferrite powder formation. The powder was calcined in a muffle furnace for three hours at 700°C.

2.3 Biosynthesis of Silver-Doped Copper Ferrite Nanoparticles

Ag-doped $CuFe_2O_4$ nanoparticles were prepared following the same procedure, with the addition of silver at different ratios. Three compositions (Ag~0.05~Cu~0.95~Fe_2O_4, Ag~0.1~Cu~0.9~Fe_2O_4, and $Ag_xCu_{1-x}Fe_2O_4$) were synthesized by adding cupric nitrate, ferric nitrate, and silver nitrate in appropriate stoichiometric ratios.

III. RESULTS AND DISCUSSION

3.1 Structural Characterization

X-ray diffraction patterns confirmed the successful formation of cubic spinel structures in all samples. Characteristic diffraction peaks appeared at 2θ values of approximately 18.3°, 30.1°, 35.5°, 43.1°, 53.4°, 57.0°, and 62.6°, corresponding to the (111), (220), (311), (400), (422), (511), and (440) crystallographic planes. The most intense peak at 35.5° corresponds to the (311) plane, typical for spinel ferrites as shown in **Figure 1**. As silver doping concentration

IJARSCT
International Journal of Advanced Research in Science, Communication and Technology
International Open-Access, Double-Blind, Peer-Reviewed, Refereed, Multidisciplinary Online Journal
ISSN: 2581-9429
Volume 5, Issue 3, July 2025
Impact Factor: 7.67

increased from 5% to 20%, notable enhancement in peak intensity and sharpness occurred, particularly in the (311) reflection, indicating improved crystallinity and larger crystallite size with higher silver content [15, 16].

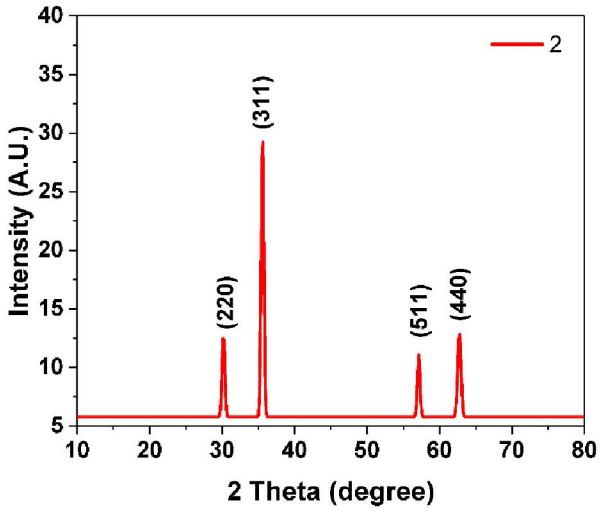

Figure 1 X-ray diffraction (XRD) patterns of $Ag_xCu_{(1-x)}Fe_2O_4$ (x=0.1) nanocomposites

The absence of additional peaks corresponding to metallic silver or silver oxide phases suggests successful incorporation of silver ions into the spinel lattice structure. The lattice parameter exhibited a non-monotonic trend, decreasing from 8.294 Å for pure $CuFe_2O_4$ to 8.270 Å for 5% silver doping, reaching a minimum of 8.165 Å at 10% silver doping, before increasing to 8.240 Å at 20% silver doping. This variation indicates complex substitution mechanisms and possible phase segregation at higher doping levels [17].

Table 2 Full width Half maximum (FWHM), Crystallite size (D) nm for $Ag_xCu_{(1-x)}Fe_2O_4$ (x= 0.1) nanoparticles

2θ	θ in Degree	Radian(θ)	FWHM Degree (θ)	FWHM Radian (θ)	Cos θ	D= 0.9λ/βCosθ	D nm
18.214	9.107	0.159	0.44791	0.008	0.987	179.74	17.97
29.899	14.949	0.261	0.45514	0.008	0.966	180.77	18.08
35.839	17.919	0.313	0.57368	0.010	0.952	145.62	14.56
37.074	18.537	0.323	0.67087	0.012	0.948	124.97	12.50
43.946	21.973	0.383	0.73111	0.013	0.927	117.24	11.72
53.926	26.963	0.470	0.38789	0.007	0.891	229.90	22.99
58.032	29.016	0.506	0.59421	0.010	0.875	152.96	15.30
63.827	31.914	0.557	1.00737	0.018	0.849	92.95	9.29
74.623	37.312	0.651	0.60665	0.011	0.796	164.71	16.47
							15.43

Crystallite sizes calculated using the Scherrer equation demonstrated considerable variation across different compositions, with average values of 15.43 nm, 15.56 nm, 16.49 nm, and 18.85 nm for undoped, 5%, 10%, and 20% silver-doped samples, respectively, suggesting that 10% silver doping promotes optimal crystal growth [18].

IJARSCT
International Journal of Advanced Research in Science, Communication and Technology
International Open-Access, Double-Blind, Peer-Reviewed, Refereed, Multidisciplinary Online Journal
ISSN: 2581-9429
Volume 5, Issue 3, July 2025
Impact Factor: 7.67

3.2 Thermal Analysis

Thermogravimetric analysis revealed a multi-stage thermal decomposition process with excellent stability. The material exhibited minimal weight loss (0.864%) up to approximately 100°C, likely attributed to desorption of physisorbed water and volatile impurities. A more significant decomposition stage occurred between 100-300°C with 5.210% weight loss, corresponding to removal of chemisorbed water, organic residues from synthesis, and possible structural hydroxyl groups. The major thermal event happened between 300-600°C with substantial 24.144% weight loss, attributed to decomposition of organic ligands, carbonaceous materials, or precursor residues, and potentially some structural rearrangement of the spinel ferrite matrix. Beyond 600°C, the material demonstrated remarkable thermal stability with only minor weight changes, indicating formation of stable Ag-doped $CuFe_2O_4$ crystalline phase.

3.3 Spectroscopic Analysis

FTIR spectra revealed characteristic vibrational modes of the spinel ferrite structure with systematic changes upon silver incorporation. All samples exhibited fundamental metal-oxygen stretching vibrations in the fingerprint region, with prominent peaks around 579-651 cm^{-1} and 419-428 cm^{-1} corresponding to tetrahedral (Fe^{3+}-O) and octahedral (Cu^{2+}/Fe^{3+}-O) site vibrations, respectively, confirming the cubic spinel structure as shown in **Figure 2**. Broad absorption bands in the 3000-3500 cm^{-1} region and around 1640 cm^{-1} were attributed to O-H stretching and bending vibrations of surface-adsorbed water molecules and hydroxyl groups [19, 20].

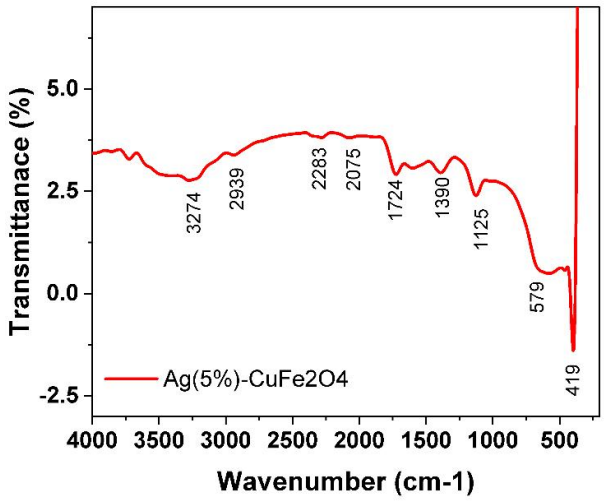

Figure 2 FTIR spectra of $Ag_xCu_{(1-x)}Fe_2O_4$ (x=0.1) showing characteristic absorption bands of the spinel ferrite structure.

UV-Vis absorption spectra demonstrated significant optical property modifications upon silver incorporation, with dramatic enhancement in absorption intensity and spectral profile changes. Pure $CuFe_2O_4$ exhibited a broad absorption band around 460 nm, characteristic of d-d transitions in Cu^{2+} and Fe^{3+} ions within the spinel structure. Upon silver doping, progressive increase in overall absorption intensity occurred along with emergence of additional absorption features. The intense absorption in the UV region (200-300 nm) can be attributed to ligand-to-metal charge transfer transitions involving silver ions and possible surface plasmon resonance effects [18, 20].

3.4 Morphological Analysis

SEM micrographs revealed distinct morphological variations in Ag~x~Cu~1-x~Fe_2O_4 nanocomposites as silver concentration increased. Pristine $CuFe_2O_4$ exhibited agglomerated spherical particles with sizes ranging from 50-200 nm, forming clustered microstructures. Upon 5% silver incorporation, the morphology became more uniform with

IJARSCT
International Journal of Advanced Research in Science, Communication and Technology
International Open-Access, Double-Blind, Peer-Reviewed, Refereed, Multidisciplinary Online Journal
ISSN: 2581-9429
Volume 5, Issue 3, July 2025
Impact Factor: 7.67

reduced agglomeration. The 10% silver-doped sample displayed well-defined crystalline facets with particle sizes between 100-500 nm, suggesting enhanced crystallinity. At 20% silver content, larger polyhedral particles emerged with distinct grain boundaries, reaching sizes up to 1 µm. This progressive morphological evolution demonstrates that silver doping significantly influences crystal growth kinetics and surface energy.

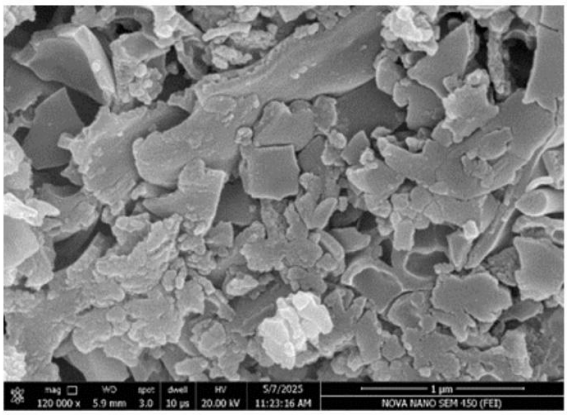

Figure 3 SEM images showing morphological changes in $Ag_xCu_{(1-x)}Fe_2O_4$ with silver doping levels of 10%

HRTEM analysis of $Ag_xCu_{(1-x)}Fe_2O_4$ revealed well-crystallized nanoparticles with distinct morphological characteristics. The particles exhibited spherical to quasi-spherical morphology with sizes ranging from 20-50 nm, demonstrating good dispersion with minimal agglomeration. Selected area electron diffraction patterns displayed bright, well-defined spots arranged in concentric rings, characteristic of polycrystalline cubic spinel structure, with distinct diffraction rings corresponding to (220), (311), (400), (511), and (440) planes.

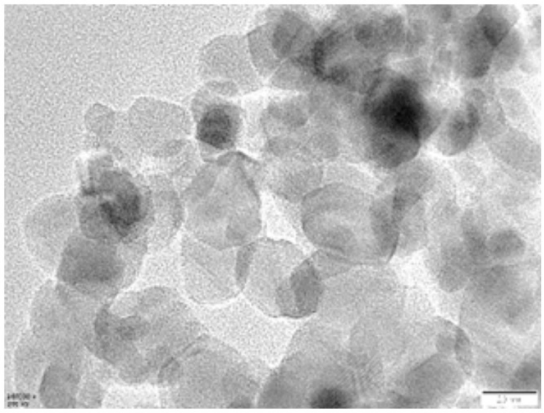

Figure 9 HRTEM micrographs of $Ag_{0.1}Cu_{0.9}Fe_2O_4$

3.5 Elemental Composition

Compositional examination demonstrated consistent elemental distribution patterns corresponding to increasing dopant concentrations. Silver incorporation escalated systematically from 5.03 wt% to 18.32 wt%, confirming effective integration within the crystalline framework. Simultaneously, oxygen composition decreased substantially from 84.49 wt% (undoped material) to 72.42 wt% (maximum silver loading), signifying considerable structural rearrangements. Iron distribution underwent dramatic alterations, declining from 12.54 wt% in the parent compound to 4.30 wt% at peak doping levels, whereas copper percentages maintained comparative stability across the 2.98-4.95 wt% range. This selective iron displacement indicates that silver cations preferentially occupy Fe^{3+} positions within the inverse spinel architecture.

IJARSCT
International Journal of Advanced Research in Science, Communication and Technology
International Open-Access, Double-Blind, Peer-Reviewed, Refereed, Multidisciplinary Online Journal
ISSN: 2581-9429
Volume 5, Issue 3, July 2025
Impact Factor: 7.67

3.6 Magnetic Properties

Magnetic characterization through vibrating sample magnetometry revealed distinctive ferrimagnetic behavior across all synthesized compositions, with notable variations in saturation magnetization values. Pure $CuFe_2O_4$ exhibited characteristic S-shaped hysteresis with saturation magnetization approaching 30 emu/g, confirming its inverse spinel structure. Silver incorporation progressively altered magnetic properties, where 5% silver-doped samples demonstrated enhanced magnetization reaching approximately 250 emu/g. However, 20% Ag- $CuFe_2O_4$ displayed reduced saturation magnetization around 85 emu/g, attributed to magnetic dilution effects where non-magnetic silver atoms disrupt magnetic exchange interactions between Fe^{3+} and Cu^{2+} ions. The narrow hysteresis loops observed across all samples indicate soft magnetic characteristics with relatively low coercive fields [21, 22].

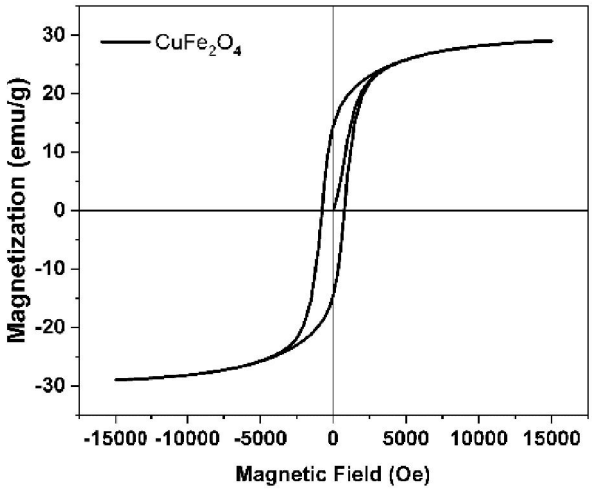

Figure 4 Vibrating Sample Magnetometry (VSM) hysteresis loops of Ag-doped $CuFe_2O_4$ nanocomposites: 10% Ag-$CuFe_2O_4$

3.7 Antimicrobial Activity

Antibiotic susceptibility tests for $CuFe_2O_4$ and all silver-doped variants were evaluated against gram-positive bacteria (*Bacillus subtilis*, *Staphylococcus aureus*) and gram-negative bacteria (*Salmonella typhimurium*, *Klebsiella pneumonia*) using disk diffusion method on Mueller-Hinton agar plates. The concentrated 100 mg samples were sonicated in distilled water and applied to individual inoculated agar plates, which were then incubated at 37°C for 24 hours. Zones of inhibition surrounding the coated samples were measured as parameters of antibacterial property [23, 24]. Results demonstrated that silver-doped samples displayed superior antimicrobial efficacy compared to undoped copper ferrite. The inhibition zones ranged from 8-19 mm across different bacterial strains, with optimal performance observed at moderate silver doping concentrations. The enhanced antimicrobial activity can be attributed to the synergistic effects between copper ferrite and silver nanoparticles, where silver ions disrupt bacterial cell membranes and interfere with cellular metabolism [25].

IJARSCT
International Journal of Advanced Research in Science, Communication and Technology
International Open-Access, Double-Blind, Peer-Reviewed, Refereed, Multidisciplinary Online Journal
ISSN: 2581-9429
Volume 5, Issue 3, July 2025
Impact Factor: 7.67

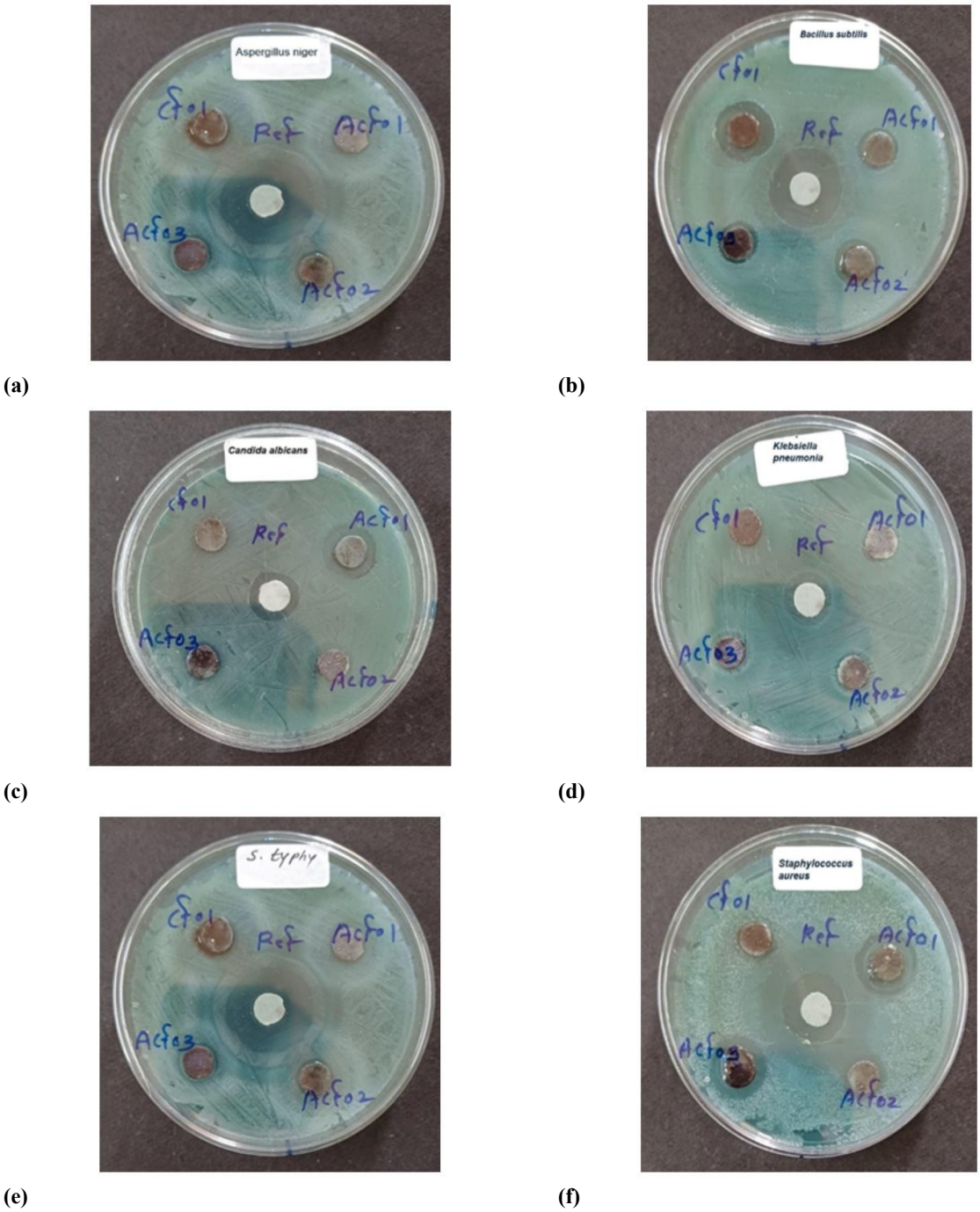

Figure 5 General bacterial strains: Antimicrobial activity of $Ag_xCu_{(1-x)}Fe_2O_4$ (x=0.05, 0.1, 0.2) nanocomposites showing zone of inhibition against different bacterial strains: (a) A. Niger, (b) B. subtilis, (c) C. Albicans, (d) K. pneumoniae, (e) S. Typhy, and (f) S. aureus.

IJARSCT
International Journal of Advanced Research in Science, Communication and Technology
International Open-Access, Double-Blind, Peer-Reviewed, Refereed, Multidisciplinary Online Journal
ISSN: 2581-9429
Volume 5, Issue 3, July 2025
Impact Factor: 7.67

3.8 Antioxidant Activity

DPPH radical scavenging assay results demonstrated marked enhancement in antioxidant properties upon silver incorporation into the copper ferrite matrix. Different concentrations (25, 50, 75, 100, and 150 µg/mL) were evaluated, with absorbance measurements revealing systematic decrease with increasing sample concentration across all formulations, indicating effective radical neutralization. The inhibition parentage of free radicals was calculated based on the formula as follows [26-28].

$$DPPH\ scavenging\ activity\ (\%)\ =\ \%\ inhibition\ Control\ =\ \frac{A_C - A_S}{A_C} \times 100 \qquad (1)$$

A_c = O.D. of Control (standard) and
A_s = O.D. of Sample

The silver-doped variants exhibited lower absorbance values compared to pristine $CuFe_2O_4$, with $Ag_xCu_{1-x}Fe_2O_4$ showing the most pronounced reduction at all tested concentrations. The calculated radical scavenging activity percentages substantiated this trend, where the highest silver-doped sample achieved 55.35% RSA at 250 mg concentration, significantly surpassing the 41.87% observed for undoped $CuFe_2O_4$. This progressive improvement correlates directly with increasing silver content, suggesting that silver dopants introduce additional electron-donating sites that facilitate DPPH radical neutralization [26-28].

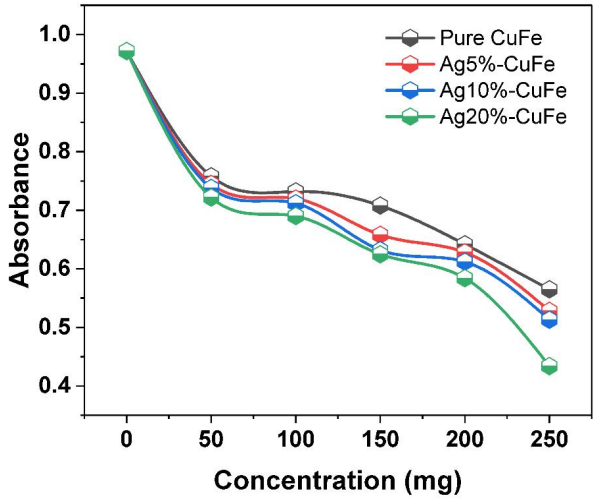

Figure 6 Comparative analysis of DPPH radical scavenging efficiency of pure and Ag-doped $CuFe_2O_4$ nanoparticles at different silver doping concentrations

The enhanced performance can be attributed to synergistic interaction between silver nanoparticles and the ferrite host, creating a more efficient electron transfer mechanism. The concentration-dependent behavior observed across all samples follows typical antioxidant kinetics, where higher material concentrations provide greater availability of active sites for radical scavenging. The silver doping effect becomes increasingly pronounced at higher concentrations, indicating that the enhanced antioxidant mechanism is dose-dependent and potentially governed by surface-mediated interactions between the nanoparticles and DPPH radicals [29, 30]..

IV. CONCLUSION

This research successfully established microwave-assisted biosynthesis of Ag-doped $CuFe_2O_4$ nanoparticles utilizing *Asteracantha longifolia* leaf extract, presenting an environmentally friendly route for developing advanced nanomaterials. Structural characterization confirmed formation of pure cubic spinel phases with silver effectively

IJARSCT
International Journal of Advanced Research in Science, Communication and Technology
International Open-Access, Double-Blind, Peer-Reviewed, Refereed, Multidisciplinary Online Journal
ISSN: 2581-9429 Volume 5, Issue 3, July 2025 Impact Factor: 7.67

integrated into the ferrite lattice without generating secondary phases. The systematic modifications in lattice parameters (8.294 to 8.165 Å) and crystallite dimensions (15.43 to 18.85 nm) demonstrate how silver incorporation influences fundamental material characteristics. Thermal analysis revealed stability up to 600°C, while optical studies showed enhanced UV-visible absorption capabilities. Biological evaluation yielded particularly promising results, with silver-doped samples displaying superior antimicrobial efficacy against both gram-positive and gram-negative bacterial strains, achieving inhibition zones of 8-19 mm. Antioxidant assessment through DPPH radical scavenging assays revealed concentration-dependent activity enhancement with silver doping, with $Ag_xCu_{1-x}Fe_2O_4$ achieving 55.35% radical scavenging activity at 250 mg concentration, substantially exceeding the 41.87% recorded for undoped copper ferrite. The combination of environmentally sustainable synthesis, structural integrity, enhanced biological activity, and improved antioxidant properties establishes these silver-doped copper ferrite nanoparticles as versatile materials for diverse applications including antimicrobial coatings, drug delivery platforms, photocatalytic systems, and environmental remediation technologies. Future work should focus on optimizing synthesis conditions and exploring additional biological applications to fully exploit their therapeutic potential.

REFERENCES

[1] A.K. Dash, G.K. Dutta, G. Sahoo, S.K. Mishra, K.K. Sardar, P.C. Bisoi, Phytochemical screening, mineral and proximate composition of Asteracantha longifolia leaf extracts as a quality livestock feed, J Med Plants Res, 6 (2012) 3786-3799.

[2] M. Kuznetsov, Y.G. Morozov, O. Belousova, Synthesis of copper ferrite nanoparticles, Inorganic materials, 49 (2013) 606-615.

[3] K. Hatami Kahkesh, Z. Baghbantaraghdari, D. Jamaledin, F. Dabbagh Moghaddam, N. Kaneko, M. Ghovvati, Synthesis, characterization, antioxidant and antibacterial activities of zinc ferrite and copper ferrite nanoparticles, Materials Chemistry Horizons, 2 (2023) 49-56.

[4] N. Phuyal, The chemical characteristics and antibacterial activity of green tea (camellia sinensis), stinging nettle (urtica diocia) leaves and the blend, Department of Microbiology, 2021.

[5] L.E. Craker, Plant alkaloids: a guide to their discovery and distribution, Routledge2018.

[6] T.S. Juthi, Studies on the Effects of Asteracantha longifolia on Retardation of Glucose Absorption and Carbohydrate Digestion in Long-Evans Rats, East West University, 2017.

[7] J.F. Setu, Evaluation of Anti–diabetic activity of Asteracantha longifolia in Long Evans Rats, East West University, 2017.

[8] S. RAO, C. ANSAR KAMRAN, PHYTOCHEMICAL ANALYSIS AND IN VITRO CYTOTOXIC ACTIVITY OF ASTERACANTHA LONGIFOLIA EXTRACT ON MCF 7 AND NIH 3T3 CANCER CELL LINES, Journal of Cell and Tissue Research, 13 (2013) 3877-3882.

[9] A.K. Shukla, R.K. Malviya, J.N. Mishra, A Review on Pharmacological Potential of Asteracantha Longifolia, International journal of health sciences, 6 14361-14369.

[10] T. Misra, R. Singh, H. Pandey, B. Singh, R. Pandey, Constituents of Asteracantha longifolia, Fitoterapia, 72 (2001) 194-196.

[11] H. Jiao, G. Jiao, J. Wang, Preparation and magnetic properties of CuFe2O4 nanoparticles, Synthesis and Reactivity in Inorganic, Metal-Organic, and Nano-Metal Chemistry, 43 (2013) 131-134.

[12] N. El Messaoudi, Z. Ciğeroğlu, Z.M. Şenol, E.S. Kazan-Kaya, Y. Fernine, S. Gubernat, Z. Lopicic, Green synthesis of CuFe2O4 nanoparticles from bioresource extracts and their applications in different areas: a review, Biomass Conversion and Biorefinery, 15 (2025) 99-120.

[13] S.A. Jasim, I. Patra, M.J.C. Opulencia, K. Hachem, R.M.R. Parra, M.J. Ansari, A.T. Jalil, M.E. Al-Gazally, M. Naderifar, M. Khatami, Green synthesis of spinel copper ferrite (CuFe2O4) nanoparticles and their toxicity, Nanotechnology Reviews, 11 (2022) 2483-2492.

[14] A.M. Mohamed, Sustainable recovery of silver nanoparticles from electronic waste: applications and safety concerns, Academia Engineering, 1 (2024).

IJARSCT
International Journal of Advanced Research in Science, Communication and Technology
International Open-Access, Double-Blind, Peer-Reviewed, Refereed, Multidisciplinary Online Journal
ISSN: 2581-9429 Volume 5, Issue 3, July 2025 Impact Factor: 7.67

[15] M. Hashemi, S. Abolghasemi, F. Rahimi, S. Rajabi, A. Nasiri, Peroxydisulfate activation by synergized modified AgCuFe2O4@ GO nanoparticle electrode with anchored MnO2 in cefixime three-dimensional electrochemical degradation: Optimization and mechanisms, Journal of Environmental Management, 373 (2025) 123978.
[16] S. Rajabi, Z. Derakhshan, S. Maleky, A. Nasiri, B. Ahmadi, M. Feilizadeh, A. Mohammadpour, M.R. Samaei, M. Hashemi, Innovative grey water treatment using eco-friendly bio-photocatalyst AgCuFe2O4@ chitosan in the presence of synergistic effects of persulfate activation: optimization and mechanisms, International Journal of Biological Macromolecules, 286 (2025) 138375.
[17] E.J. Abdelrazek, A.A. Gahlan, G.A. Gouda, A.S. Ahmed, Cost-effective adsorption of cationic dyes using ZnO nanorods supported by orange peel-derived carbon, Scientific Reports, 15 (2025) 4123.
[18] M. Sangeetha, S. Ambika, D. Madhan, S. Vadivel, Photocatalytic activity of Ag doped CuFe2O4 nanoparticles supported on reduced graphene oxide for the degradation of organic dyes under visible light irradiation, Journal of Materials Science: Materials in Electronics, 35 (2024) 368.
[19] M. Pourshaban-Mazandarani, A. Nasiri, Photocatalytic degradation of tetracycline in wastewater with bio-based matrix magnetic heterogeneous nanocatalyst: performance and mechanism study, Journal of Polymers and the Environment, 32 (2024) 5713-5737.
[20] Z. Zhu, X. Li, Q. Zhao, Y. Li, C. Sun, Y. Cao, Photocatalytic performances and activities of Ag-doped CuFe2O4 nanoparticles, Materials Research Bulletin, 48 (2013) 2927-2932.
[21] A. Pawar, B. Patil, S. Bhongale, A. Salunkhe, S. Kumar, T. Shinde, Effect of Ag doping on DC electrical resistivity, thermoelectrical power, VSM analysis and antimicrobial activity of copper-zinc nano-ferrites, Indian Journal of Physics, 96 (2022) 3161-3176.
[22] S.M. Rathod, A.R. Chavan, S.S. Jadhav, K.M. Batoo, M. Hadi, E.H. Raslan, Ag+ ion substituted CuFe2O4 nanoparticles: Analysis of structural and magnetic behavior, Chemical Physics Letters, 765 (2021) 138308.
[23] S. Kalia, V. Dhiman, N. Prasad, Unveiling the integrated characteristics of Cu–Ag co-doped CoFe2O4: Structural, morphological, magnetic, and antibacterial perspectives, Materials Chemistry and Physics, 334 (2025) 130417.
[24] K. Atacan, M. Özacar, M. Özacar, Investigation of antibacterial properties of novel papain immobilized on tannic acid modified Ag/CuFe2O4 magnetic nanoparticles, International journal of biological macromolecules, 109 (2018) 720-731.
[25] H. Fujikawa, M. Matsushita, Fractal growth of Bacillus subtilis on agar plates, Journal of the physical society of japan, 58 (1989) 3875-3878.
[26] İ. Gulcin, S.H. Alwasel, DPPH radical scavenging assay, Processes, 11 (2023) 2248.
[27] S.B. Kedare, R. Singh, Genesis and development of DPPH method of antioxidant assay, Journal of food science and technology, 48 (2011) 412-422.
[28] M.C. Foti, Use and Abuse of the DPPH• Radical, Journal of agricultural and food chemistry, 63 (2015) 8765-8776.
[29] K.H. Musa, A. Abdullah, A. Al-Haiqi, Determination of DPPH free radical scavenging activity: application of artificial neural networks, Food chemistry, 194 (2016) 705-711.
[30] N. Nenadis, M. Tsimidou, Observations on the estimation of scavenging activity of phenolic compounds using rapid 1, 1-diphenyl-2-picrylhydrazyl (DPPH•) tests, Journal of the American Oil Chemists' Society, 79 (2002) 1191-1195.